HHS Public Access

Author manuscript

J Nucl Med. Author manuscript; available in PMC 2016 March 01.

Published in final edited form as:

J Nucl Med. 2015 March ; 56(3): 483–488. doi:10.2967/jnumed.114.146605.

Cerenkov specific contrast agents for detection of pH in vivo

Julie Czupryna, **Alexander V. Kachur**, **Eric Blankemeyer**, **Anatoliy V. Popov**, **Joel S. Karp**, and **E. James Delikatny***

Small Animal Imaging Facility, Department of Radiology, Perelman School of Medicine, University of Pennsylvania

Abstract

We report the design, testing and in vivo application of pH sensitive contrast agents designed specifically for Cerenkov imaging. Radioisotopes used for positron emission tomography (PET) emit photons via Cerenkov radiation. The multispectral emission of Cerenkov radiation allows for selective bandwidth quenching, where a band of photons are quenched by absorption by a functional dye. Under acidic conditions, ^{18}F-labeled derivatives emit the full spectrum of Cerenkov light. Under basic conditions, the dyes change color and a wavelength-dependent quenching of Cerenkov emission is observed.

METHODS—Mono and di-^{18}F-labeled derivatives of phenolsulfonphthalein (phenol red) and *meta*-cresolsulfonphthalein (cresol purple) were synthesized by electrophilic fluorination. Cerenkov emission was measured at different wavelengths as a function of pH in vitro. Intramolecular response was measured in fluorinated probes; intermolecular quenching by mixing phenolphthalein with ^{18}F FDG. Monofluorocresol purple (MFCP) was tested in mice treated with acetazolamide to cause urinary alkalinization and Cerenkov images compared to PET images.

RESULTS—Fluorinated pH indicators were produced with radiochemical yields of 4-11% at >90% purity. Selective Cerenkov quenching was observed intramolecularly with difluorophenol red or MFCP, and intermolecularly in phenolphthalein ^{18}F-FDG mixtures. The probes were selectively quenched in the bandwidth closest to the indicator's absorption maximum (λ_{max}) at pHs above the indicator pKa. Addition of acid or base to the probes resulted in reversible switching from unquenched to quenched emission. In vivo, the bladders of acetazolamide-treated mice exhibited a wavelength-dependent quenching in Cerenkov emission, with the greatest reduction occurring near the λ_{max}. Ratiometric imaging at two wavelengths showed significant decreases in Cerenkov emission at basic pH and allowed the estimation of absolute pH in vivo.

CONCLUSIONS—We have created contrast agents that selectively quench photons emitted during Cerenkov radiation within a given bandwidth. In the presence of a functional dye, such as a pH indicator, this selective quenching allows for a functional determination of pH in vitro and in vivo. This method can be used to obtain functional information from radiolabeled proves using multimodal imaging. It allows for the imaging of *non-fluorescent* chromophores and is generalizable to any functional dye that absorbs at suitable wavelengths.

* Corresponding Author: James Delikatny, Ph.D., 317 Anatomy Chemistry Building, 3620 Hamilton Walk, Philadelphia, PA 19104, Phone: (215) 898-3105; Fax: (215) 746-8764; delikatn@mail.med.upenn.edu.

Keywords

Cerenkov imaging; ratiometric imaging; pH measurement; electrophilic fluorination; metacresol purple; phenolphthalein

INTRODUCTION

Cerenkov imaging (CI) is a recently described imaging modality that detects photons emitted by radioactive particles during beta decay. Cerenkov radiation (CR) arises when charged particles exceed the speed of light when traveling through a dielectric medium and is the source of the blue light emitted by nuclear reactors. CR was described by Pavel Cerenkov, for which he won the 1958 Nobel Prize with Frank and Tamm (*1, 2*). However, the potential for CI was not recognized until 2009 when the first small animal study was published (*3*).

CI can be accomplished using standard optical imaging equipment, detecting the photons using a cooled, charge-couple device (CCD) camera. This allows for high throughput (3-5 animals per scan in optical scanners) with scan times that are often less than 5 minutes (*4, 5*). In addition, any β-emitter, positron or electron, can be imaged, allowing for CI of nuclei such as ^{32}P (*6*).

Most Cerenkov photons are in the visible range, and as a result are subject to tissue absorption and scattering, limiting the depth of detection. While more suited for small animal applications, CI also has the potential for human imaging. Cerenkov studies of ^{131}I in human thyroid (*7*) and ^{18}F-fluorodeoxyglucose (^{18}F-FDG) in positive lymph nodes from cancer patients (*8*) have recently been published. Future human use will most likely be restricted to surface tumors or tumors accessible endoscopically (*9, 10*). Many breast tumors present close to the surface and the breast is both compressible and has good optical properties, making this a potential target (*11-14*). Intraoperative use is also possible, and other groups are pursuing this approach (*15-17*).

Importantly, β^+-decay leads to the generation of 2 types of photons, the high-energy 511 keV gamma rays released after positron annihilation and detectable by PET, and the visible photons released as CR. These properties allow for the development of multimodal PET-CI tracers (*18-21*). Current radiotracer methods detect primarily location of the radioisotope, it is difficult to assess probe metabolism directly. However, CI is an optical technique and the photons can be selectively quenched or transferred to higher wavelengths (*22-24*). This allows for the creation of contrast agents where function can be measured optically while binding, kinetics and location can be followed with PET.

This paper describes Cerenkov contrast agents (*25-28*) based on the concept of selective bandwidth quenching (*28*). Cerenkov light is emitted continuously across the visible spectrum with intensity proportional to the inverse square of the wavelength, $1/\lambda^2$. A change in absorption by a functional chromophore, such as a fluorinated pH indicator becoming basic, reduces Cerenkov emission across a selective bandwidth, resulting in an attenuated signal.

We previously reported the synthesis of fluoroderivatives of the pH indicators phenolsulfonphthalein (Phenol Red, PR) (*26*), *meta*-cresolsulfonphthalein (Cresol Purple, CP) (*27*) and phenolphthalein (PP) (*25*). Here we show that the ^{18}F-isotopomers can serve as noninvasive pH probes for CI. We report ^{18}F-radiolabeling of CP and PR derivatives (Figure 1), in vitro testing and in vivo measurement of pH in a mouse model of urinary alkalinization. The principle of selective bandwidth quenching is demonstrated intermolecularly using PP mixed with ^{18}F-FDG and intramolecularly using fluorinated PR and CP. The quenching is shown to be reversible and pH dependent. Finally ^{18}F-labeled CP is used to estimate pH in the bladders of mice treated with acetazolamide, a carbonic anhydrase inhibitor. Ratiometric imaging is employed at different wavelengths to determine absolute pH values in vivo. These results provide methods for multispectral optical imaging of nonfluorescent molecules with the potential for dual measurement of function and location using radiolabeled probes.

MATERIALS AND METHODS

All reagents were purchased from Sigma-Aldrich unless otherwise stated. ^{18}F-FDG and ^{18}F-NaF were obtained from the Cyclotron Facility at the University of Pennsylvania.

^{18}F labeling

Labeling was performed using a custom-made electrophilic fluorination unit as previously described (*25-27*). ^{18}F-F_2 gas was prepared by the ^{20}Ne(d,α)^{18}F reaction using an IBA 18/9 Cyclone accelerator. ^{18}F-F_2 gas (0.1% in Ne, Matheson Tri-Gas Inc) with a total activity of 100-200 mCi in 35 μmoles of $^{19}F_2$ carrier, was bubbled for 5 minutes through a freshly prepared solution of the equivalent amount of the monosodium salt of the indicator in glacial acetic acid (2 mg/mL). The mixture was evaporated under vacuum at 120 °C, redissolved in 2 mL of water, injected onto a semi-preparative HPLC column (Phenomenex, Synergi 4 μm Hydro-RP 80 Å 10x250 mm) and eluted with 25% ethanol-water buffer at 2 mL/min with detection of radioactivity and absorption at 430 nm. Fractions corresponding to fluorinated products were collected, evaporated to dryness, and redissolved in saline for further application. An average (n=5) radiochemical yield was 4±1% for monofluorinated (MFPR), 7±1% difluorinated (DFPR), and 1±0.5% trifluorinated (TFPR) derivatives. For CP (n=9) the radiochemical yields were 9.6±1% for monofluorinated (MFCP), 11±0.7% for difluorinated (DFCP), and 4.2±0.7% for trifluorinated (TFCP). In both cases we were able to detect small amounts of tetrafluorinated derivatives. The specific activity at the time of experiment was 1-2 Ci/mmol for monofluorinated and 2-4 Ci/mmol difluorinated derivatives respectively. The purity of the probes was >90% by analytical HPLC. Analytical HPLC for DFPR and NMR data for MFCP have been published [26,27].

In vitro Cerenkov imaging

Optical imaging was performed on a PerkinElmer IVIS Lumina II. For open filter measurements, an exposure time of 30 seconds was used with large binning and f/stop=1. For selective emission filter measurements, the exposure time was 60 seconds. The Lumina has 4 emission filters with wavelengths 515-575, 575-650, 695-770 and 810-875 nm. The heater plate was set to room temperature to minimize evaporation. Black walled 96-well

plates (BD Biosciences) were filled with 200 μL of probe at the indicated activities and concentrations. For pH imaging, the pH of the solution was adjusted using 0.1 M acetate (pH 4-5.5), MES (pH 5.5-6.5), phosphate (pH 6.5-8), Trizma (pH 8-9), borate (pH 9-10) or carbonate (pH 10-11) buffers. For switching experiments, the pH was adjusted using 1M HCl or NaOH. For phantom experiments, a 1-cm^3 acrylic phantom (Data Spectrum Corporation) was filled with ^{18}F-FDG and imaged under the same conditions. Image quantification was performed using Living Image software (PerkinElmer) by drawing regions of interest (ROIs) around each well and determining the radiance. A radioactive decay constant was applied to all data except for pH switching experiments to account for the time between plating and imaging.

In vitro APET imaging

Following optical imaging, plates were centered in the FOV of the MOSAIC HP small animal APET scanner (*29*) (Philips Medical Systems) and imaged statically for 15 minutes. Images were reconstructed with a 3D Row Action Maximum Likelihood Algorithm (3D-RAMLA) (*30*). Corrections for decay, scatter, and attenuation were applied using a ^{137}Cs source. Absolute quantification of activity from the dose calibrator was achieved with cross-calibration of phantom measurements to provide nCi/mL.

In vivo Cerenkov imaging

All experiments were approved by our Institutional Animal Care and Use Committee. For ^{18}F-FDG, 4-6 week old nude mice (NCI) received ~435 μCi of ^{18}F-FDG i.v. via tail vein. For pH experiments, mice received 160 mg/kg acetazolamide (X-Gen Pharmaceuticals) in saline or saline i.p. for 5 days. On day 5, urine was collected and pH determined using an Accumet pH meter. Four hours later, mice were injected i.v. with ~400 μCi ^{18}F-MFCP. Thirty minutes later, mice were imaged using the IVIS Lumina II under 1.5% isoflurane/oxygen anesthesia using the following parameters: Open filter – Exposure time: 1 minute, Binning: Large, f/stop: 1; Selective Emission filters – Exposure time: 5 minutes. Image quantification was performed by drawing ROIs and determining the radiance. Optical data were corrected for radioactive decay to account for loss in activity and then normalized to the APET images by dividing the radiance by the PET counts in the same ROI to account for injection efficiency.

In vivo APET imaging

Subsequent to ^{18}F-MFCP injection, each mouse was imaged statically in the MOSAIC HP small animal PET scanner for 15 minutes. The images were reconstructed as described above using a voxel size of 0.5 × 0.5 × 0.5 mm^3. Decay, scatter, and attenuation correction was applied. All activity is assumed to be inside the mouse for purposes of calculation of activity concentration since we monitored the excreted activity from the mouse.

RESULTS

Initial experiments were performed to characterize Cerenkov emission in vitro and in vivo using different emission filters (Supplemental Information). A strong linear correlation was observed between optical and APET signals (Figure S1). Selective emission filters showed

that the bulk of the photons were emitted at lower wavelengths (515-575 and 575-650 nm, Figure S2 and S3B) and the emission spectrum followed the expected $1/\lambda^2$ dependence (Figure S3B). Importantly, the emission spectrum exhibited different characteristics when CR was examined in vivo. Mice imaged following administration of ^{18}F-FDG showed a marked decrease in Cerenkov intensity using the lowest wavelength (515-575 nm) filter, due to attenuation and scattering by tissue at these wavelengths (Figure S4).

To design Cerenkov specific contrast agents, intermolecular quenching of CR was first measured using PP, which is colorless when acidic (λ_{acidic}=276 nm) and fuchsia when basic (pK_a=9.8, λ_{basic}=553 nm, Figure 1). Mixing 100 μCi of ^{18}F-FDG with 25 mM PP led to a pH-dependent quenching of CR when the open, 515-575 and 575-650 nm filters were used (Figure 2A). Quenching was less pronounced in the remaining filters and the signal was much lower in the 810-875 nm range reflecting the reduced photon emission at these wavelengths.

To demonstrate intramolecular quenching, ^{18}F-labeled derivatives of a series of pH indicators were synthesized (*25-27*). The properties of 10 of these indicators are presented in Table 1. For further investigation we first selected difluorinated phenol red (DFPR, Figure 1), which exhibits a yellow (acidic) to red (basic) transition. ^{18}F-DFPR (pK_a=6.4, λ_{acidic}=428 nm, λ_{basic}=570 nm) was examined in the pH range 4-7. Figure 2B shows selective CR quenching occurred at basic pH when the open, 515-575 and 575-650 nm filters were employed, with the greatest quenching observed near λ_{basic}.

^{18}F-DFPR exhibited less of a pH dependent effect than PP and the quenching plateaued at pH > 6, leading to little overall change in the Cerenkov emission. Thus, we examined ^{18}F-labeled monofluorinated cresol purple (^{18}F-MFCP, pK_a=7.5, λ_{acidic}=440 nm, λ_{basic}=582 nm, Figure 1), which is yellow when acidic and purple under basic conditions. As shown in Figure 2C, ^{18}F-MFCP quenches Cerenkov emission in the open, 515-575 and 575-650 nm filters as pH increases. Quantification of the images is shown in Figure 2D-F. Only the open and 515-575 nm (PP+^{18}F, ^{18}F-DFPR) or 575-650 nm (^{18}F-MFCP) filters are shown as they exhibited the greatest change in CR over the pH range. ^{18}F-MFCP shows the greatest pH dependent changes in Cerenkov emission (2.7 as compared to 1.9 fold for ^{18}F-DFPR and 2.5 fold for intermolecular PP) with a pK_a relevant for in vivo studies. Quantification of the remaining filter sets is shown in Figure S5.

Intermolecular quenching of CR was shown to be switchable by adding acid or base to wells containing 25 mM PP and 100 μCi ^{18}F-FDG (Figure 3A). Intramolecular switching was also observable with either of the fluorinated indicators, ^{18}F-MFCP and ^{18}F-DFPR (Figure 3B-C). Quantification of these images (Figure 3D-F) demonstrates that for PP, the greatest change was seen using the open filter or filters at wavelengths closest to the λ_{max} (515-575 and 575-650 nm; Figure 3D). Both ^{18}F-DFPR and ^{18}F-MFCP exhibited similar characteristics (Figure 3E-F), with maximum switching observed near the λ_{max} of the chromophores.

To test ^{18}F-MFCP in vivo, nude mice were treated with acetazolamide (160 mg/kg, i.p.) or PBS for 5 days. On day 6, mouse urine was collected and pH measured. The urine of PBS-

treated mice had a pH of 6.2±0.1 (n=3), while acetazolamide-treated mice had a urine pH of 8.5±0.2 (n=3). Mice were administered ^{18}F-MFCP and imaged optically 30 minutes later followed by APET imaging. The APET images show probe accumulation in gall bladder, liver, intestine and bladder (Figure 4A). When normalized to dose injected per animal, a difference of less than 5% was observed in the average SUVs from bladders of PBS- and acetazolamide-treated mice (1.443±0.405 vs 1.444±0.471 respectively). Optical images taken using the open filter show a brighter signal in the PBS-treated mouse bladder compared to the acetazolamide-treated animal (Figure 4B). When the remaining filters were employed, the greatest difference between PBS- and acetazolamide-treated animals occurred using the 575-650 nm filter (Figure 4C) consistent with the λ_{basic}=582 nm for ^{18}F-MFCP. The images were quantified by correcting the average radiance for decay to the injection time of the tracer and normalizing to mean PET counts. Open filter images showed a decrease in acetazolamide-treated mice just outside the level of significance (Figure 5A, p=0.07). Quantification of the selective filter sets (Figure 5B) showed non-significant decreases with the greatest difference observed again using the 575-650 nm filter. Emissions at wavelengths outside the absorbance range of MFCP were not affected by acetazolamide treatment.

Ratiometric calculations were performed by taking emission for each filter relative to 810-875 nm, which was invariant to pH changes and where the greatest light penetration is expected. This resulted in a significant difference between acetazolamide and PBS-treated mice for the 575-650 (p=0.01, Students t-test) and 695-770 (p=0.02), but not for 515-575 nm filters (p=0.47, Figure 5C). A ratiometric pH response curve was created from in vitro ^{18}F-MFCP data using Cerenkov emission at 575-650 nm, where the greatest pH response was observed, relative to 810-875 nm (Figure 5D). A fit to a sigmoidal curve gave a pK_a=6.25, R^2=0.956. The in vivo ratios from control and acetazolamide treated mice were plotted against ex vivo urine pH. The in vivo ratios predicted absolute pH with reasonable accuracy, although the values tended to lie above the curve (Figure 5D).

DISCUSSION

In this paper we describe the synthesis, in vitro characterization and in vivo testing of ^{18}F-labeled pH indicators designed to exploit the characteristics of CR. The multispectral nature of Cerenkov emission allows for selective quenching of a band of photons by a functional chromophore that is used to report on pH.

The biological manifestations of pH modulation are numerous and significant. From reduced pH in lysosomes (*31*) to reduced pH in the extracellular space of tumors (*32, 33*), multimodal in vivo pH sensors could have considerable impact on the field of molecular imaging. Our approach differs from other methods of measuring pH (*34*) in that we are directly monitoring the absorption of colorimetric pH indicators, which is a standard method of pH determination. While optical imaging agents that emit in the near infrared range are preferred for in vivo imaging (*35*), the bulk of the Cerenkov signal is located near the blue end of the visible spectrum (*3, 36*). To create a balance between available signal and adequate penetration of light through tissue, pH-responsive CI probes were developed to exhibit selective bandwidth quenching in the 575-650 nm range. Our initial mouse studies

showed that although we could detect ^{18}F-FDG in nude mice using all of the emission filters, the Cerenkov emission using the 515-575 nm filter was markedly lower than the 575-650 nm filter, due to photon absorption and scattering at shorter wavelengths.

The common pH indicator, PP (λ_{max}=553 nm) was used to demonstrate intermolecular CR quenching. Wavelength-dependent quenching of CR was observed to be the most effective at 515-575 nm in the pH range 4-11 with relatively little quenching seen outside the absorption range of PP. However, PP could not quench CR in our target bandwidth of 575-650 nm and the pH necessary for quenching (>9) was not biologically relevant.

Intermolecular quenching of CR has also been shown in vivo using nanoparticles (*37*). However, intramolecular quenching would ultimately be more useful as it would require a single contrast injection. As a result ^{18}F-DFPR, a derivative of the pH indicator commonly used in cell culture, was synthesized. Quenching could be now observed in both the 515-575 nm and the target bandwidth of 575-650 nm. Although ^{18}F-DFPR could effectively quench CR, a relatively small difference in emission was observed between acidic and basic forms. Thus we synthesized ^{18}F-MFCP and found that it outperformed ^{18}F-DFPR and PP in the magnitude of quenching in the target bandwidth.

In addition selectively quenching a targeted bandwidth, it was critical that the sensors be switchable in order to accurately reflect the surrounding environment. The sequential addition of base and acid to ^{18}F-MFCP led to stepwise quenching and restoration of CI, respectively. While ^{18}F-MFCP exhibited the highest potential as an in vivo probe, we also investigated PP+^{18}F-FDG and ^{18}F-DFPR and found that they were both capable of switching. These results indicate that it is possible to rapidly monitor pH changes dynamically in the extracellular tumor space of the tumor microenvironment.

In vivo experiments were carried out using ^{18}F-MFCP in a mouse model of urinary alkalization. Acetazolamide is a carbonic anhydrase inhibitor that is used to treat metabolic and respiratory alkalosis. In doing so, it causes blood acidification and urinary alkalization. The latter property, along with the collection of small molecule radiopharmaceuticals in urine due to renal clearance, provided a model to test how well ^{18}F-MFCP reports on in vivo pH. Using a pH meter, mouse urine pH was measured to be 6.2±0.1 in controls and 8.5±0.2 in acetazolamide treated animals. Optical images of the bladder obtained following ^{18}F-MFCP administration showed a clear difference in CR output between the two experimental conditions whereas no difference in PET signal was seen. Control animals exhibited a brighter signal than acetazolamide treated animals, with the greatest difference seen in the open and 575-650 nm filter images. Following imaging, expelled urine from acetazolamide treated animals was dark purple (not shown), indicating further that the urine was basic as measured by ^{18}F-MFCP.

When ROIs around the bladder were quantified, the differences were not significant unless ratios were taken relative to the invariant signal at 810-875 nm. Using the ratiometric method, it is possible for ^{18}F-MFCP to report on absolute pH. We constructed a normalized pH response curve using in vitro ^{18}F-MFCP data by taking the ratio of emission at 575-650 to 810-875 nm. When the same ratios from the control and acetazolamide treated mice were

plotted on the pH response curve, the CR values correlated well, although they tended to lie above the curve and underestimate the actual pH. This effect may arise from scattering or absorption of light at different wavelengths, which would not contribute to the in vitro data. It is interesting to note that the pK_a for ^{18}F-MFCP as determined by Cerenkov emission in vitro (6.2) is lower than the pK_a measured using absorption (7.2). The reason for this is uncertain, although similar effects were observed for ^{18}F-DFCR and ^{18}F-PP mixed with FDG.

CONCLUSIONS

We have demonstrated the ability to image pH using selective bandwidth quenching of Cerenkov specific contrast agents. In vivo results show that ^{18}F-MFCP is capable of reporting pH in animal models. This opens a number of possibilities because it allows for direct imaging of visible chromophores. The concept of selective bandwidth quenching is generalizable to other dyes that alter their absorption in response to chemical or physiological stimuli and that absorb at wavelengths appropriate for CI. These concepts define a method for the functional imaging of non-fluorescent chromophores that could be used in conjunction with PET.

Supplementary Material

Refer to Web version on PubMed Central for supplementary material.

ACKNOWLEDGEMENTS

Supported by a Transdisciplinary Awards Program in Translational Medicine and Therapeutics-Translational Biomedical Imaging Core (TAPITMAT-TBIC) grant through UL1RR024134 and R01EB018645-01 (EJD).

REFERENCES

1. Tamm IE. General characteristics of Vavilov-Cherenkov radiation. Science. 1960; 131:206–210. [PubMed: 17732684]
2. Cherenkov PA. Radiation from high-speed particles. Science. 1960; 131:136–142. [PubMed: 13809644]
3. Robertson R, Germanos MS, Li C, Mitchell GS, Cherry SR, Silva MD. Optical imaging of Cerenkov light generation from positron-emitting radiotracers. Phys Med Biol. 2009; 54:N355–365. [PubMed: 19636082]
4. Liu H, Ren G, Miao Z, et al. Molecular optical imaging with radioactive probes. PLoS One. 2010; 5:e9470. [PubMed: 20208993]
5. Aweda TA, Eskandari V, Kukis DL, et al. New covalent capture probes for imaging and therapy, based on a combination of binding affinity and disulfide bond formation. Bioconjug Chem. 2011; 22:1479–1483. [PubMed: 21755984]
6. Spinelli AE, Kuo C, Rice BW, et al. Multispectral Cerenkov luminescence tomography for small animal optical imaging. Opt Express. 2011; 19:12605–12618. [PubMed: 21716501]
7. Spinelli AE, Ferdeghini M, Cavedon C, et al. First human Cerenkography. J Biomed Opt. 2013; 18:20502. [PubMed: 23334715]
8. Thorek DL, Riedl C, Grimm J. Clinical Cerenkov luminescence imaging of 18F-FDG. J Nucl Med. 2013; 55:95–98. [PubMed: 24078721]
9. Zhang JG, Liu HF. Functional imaging and endoscopy. World J Gastroenterol. 2011; 17:4277–4282. [PubMed: 22090783]

10. Kothapalli SR, Liu H, Liao JC, Cheng Z, Gambhir SS. Endoscopic imaging of Cerenkov luminescence. Biomed Opt Express. 2012; 3:1215–1225. [PubMed: 22741069]
11. Corlu A, Choe R, Durduran T, et al. Three-dimensional in vivo fluorescence diffuse optical tomography of breast cancer in humans. Opt Express. 2007; 15:6696–6716. [PubMed: 19546980]
12. Durduran T, Choe R, Yu G, et al. Diffuse optical measurement of blood flow in breast tumors. Opt Lett. 2005; 30:2915–2917. [PubMed: 16279468]
13. Tromberg BJ, Pogue BW, Paulsen KD, Yodh AG, Boas DA, Cerussi AE. Assessing the future of diffuse optical imaging technologies for breast cancer management. Med Phys. 2008; 35:2443–2451. [PubMed: 18649477]
14. Boverman G, Fang Q, Carp SA, et al. Spatio-temporal imaging of the hemoglobin in the compressed breast with diffuse optical tomography. Phys Med Biol. 2007; 52:3619–3641. [PubMed: 17664563]
15. Liu H, Carpenter CM, Jiang H, et al. Intraoperative imaging of tumors using Cerenkov luminescence endoscopy: a feasibility experimental study. J Nucl Med. 2012; 53:1579–1584. [PubMed: 22904353]
16. Holland JP, Normand G, Ruggiero A, Lewis JS, Grimm J. Intraoperative imaging of positron emission tomographic radiotracers using Cerenkov luminescence emissions. Mol Imaging. 2011; 10:177–186. 171-173. [PubMed: 21496448]
17. Thorek DL, Abou DS, Beattie BJ, et al. Positron lymphography: multimodal, high-resolution, dynamic mapping and resection of lymph nodes after intradermal injection of 18F-FDG. J Nucl Med. 2012; 53:1438–1445. [PubMed: 22872741]
18. Robertson R, Germanos MS, Manfredi MG, Smith PG, Silva MD. Multimodal imaging with 18F-FDG PET and Cerenkov luminescence imaging after MLN4924 treatment in a human lymphoma xenograft model. J Nucl Med. 2011; 52:1764–1769. [PubMed: 21994410]
19. Ruggiero A, Holland JP, Lewis JS, Grimm J. Cerenkov luminescence imaging of medical isotopes. J Nucl Med. 2010; 51:1123–1130. [PubMed: 20554722]
20. Li C, Mitchell GS, Cherry SR. Cerenkov luminescence tomography for small-animal imaging. Opt Lett. 2010; 35:1109–1111. [PubMed: 20364233]
21. Natarajan A, Habte F, Liu H, et al. Evaluation of Zr-rituximab Tracer by Cerenkov luminescence imaging and correlation with PET in a humanized transgenic mouse model to image NHL. Mol Imaging Biol. 2013; 15:468–475. [PubMed: 23471750]
22. Dothager RS, Goiffon RJ, Jackson E, Harpstrite S, Piwnica-Worms D. Cerenkov radiation energy transfer (CRET) imaging: a novel method for optical imaging of PET isotopes in biological systems. PLoS One. 2010; 5:e13300. [PubMed: 20949021]
23. Kotagiri N, Niedzwiedzki DM, Ohara K, Achilefu S. Activatable probes based on distance-dependent luminescence associated with Cerenkov radiation. Angew Chem Int Ed Engl. 2013; 52:7756–7760. [PubMed: 23765506]
24. Axelsson J, Davis SC, Gladstone DJ, Pogue BW. Cerenkov emission induced by external beam radiation stimulates molecular fluorescence. Med Phys. 2011; 38:4127–4132. [PubMed: 21859013]
25. Kachur AV, Popov AA, Delikatny EJ, Karp JS, Popov AV. Synthesis of 18F-labeled phenolphthalein and naphtholphthalein. J Fluorine Chem. 2013; 151:1–6.
26. Kachur AV, Popov AV, Karp JS, Delikatny EJ. Direct fluorination of phenolsulfonphthalein: a method for synthesis of positron-emitting indicators for in vivo pH measurement. Cell Biochem Biophys. 2013; 66:1–5. [PubMed: 22790882]
27. Kachur AV, Sardelis D, Bentzley C, Popov AV, Delikatny EJ, Karp JS. Synthesis and characterization of fluorinated derivatives of cresolsulfonphthalein. J Fluorine Chem. 2013; 145:112–117.
28. Czupryna J, Kachur AV, Blankemeyer E, Popov AV, Karp JS, Delikatny EJ. In vivo pH detection using switchable 18F labeled Cerenkov probes [abstract]. J Nucl Med. 2012; 53(Supp 1):73.
29. Surti S, Karp JS, Perkins AE, et al. Imaging performance of A-PET: a small animal PET camera. IEEE Trans Med Imaging. 2005; 24:844–852. [PubMed: 16011313]

30. Daube-Witherspoon ME, Matej S, Karp JS, Lewitt RM. Application of the Row Action Maximum Likelihood Algorithm with spherical basis functions to clinical PET imaging. IEEE Trans Med Imaging. 2001; 48:24–30.

31. Mindell JA. Lysosomal acidification mechanisms. Annu Rev Physiol. 2012; 74:69–86. [PubMed: 22335796]

32. Robey IF, Baggett BK, Kirkpatrick ND, et al. Bicarbonate increases tumor pH and inhibits spontaneous metastases. Cancer Res. 2009; 69:2260–2268. [PubMed: 19276390]

33. Hashim AI, Zhang X, Wojtkowiak JW, Martinez GV, Gillies RJ. Imaging pH and metastasis. NMR Biomed. 2011; 24:582–591. [PubMed: 21387439]

34. Zhang X, Lin Y, Gillies RJ. Tumor pH and its measurement. J Nucl Med. 2010; 51:1167–1170. [PubMed: 20660380]

35. Ntziachristos V, Bremer C, Weissleder R. Fluorescence imaging with near-infrared light: new technological advances that enable in vivo molecular imaging. Eur Radiol. 2003; 13:195–208. [PubMed: 12541130]

36. Park JC, Il An G, Park SI, et al. Luminescence imaging using radionuclides: a potential application in molecular imaging. Nucl Med Biol. 2011; 38:321–329. [PubMed: 21492780]

37. Thorek DL, Das S, Grimm J. Molecular imaging using nanoparticle quenchers of Cerenkov luminescence. Small. 2014; 10:3729–3734. [PubMed: 24861843]

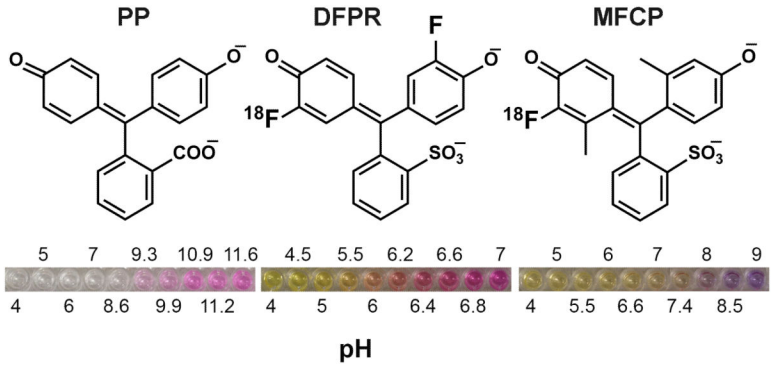

Figure 1. Chemical structures of the pH indicators

Left: phenolphthalein (PP); Middle: difluorophenol red (DFPR); Right: monofluorocresol purple (MFCP). The pH dependent changes in the indicator color is shown underneath.

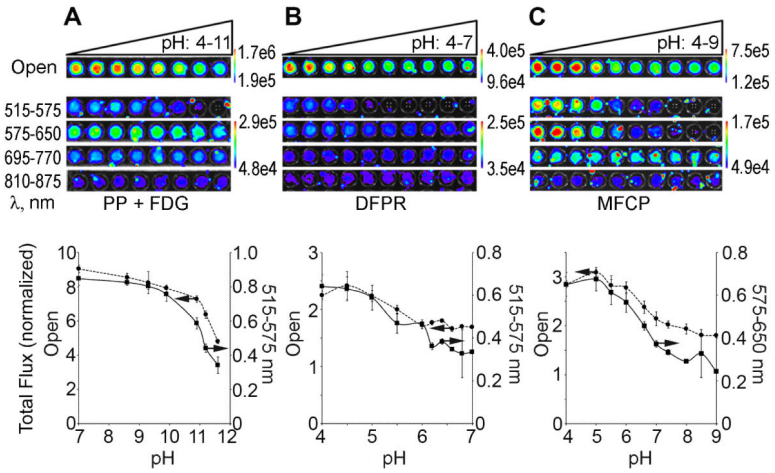

Figure 2. Inter- and intramolecular quenching of Cerenkov radiation

(A) 25 mM PP was adjusted to pH 4-11, mixed with 100 μCi ^{18}F-FDG and imaged using all filters on the IVIS Lumina II. The top panel shows images of the plate and the bottom panel quantifications of total flux normalized to APET counts for the open filter (dashed line) and optimal quenching 515-575 nm filter (solid line). (B) 100 μCi (25 nmol) ^{18}F-DFPR adjusted to pH 4-7 with the open and 515-575 nm filters quantification shown (C) 140 μCi (70 nmol) ^{18}F-MFCP adjusted to pH 4-9 with the open and 575-650 nm filters. For each pH indicator, the filtered images were set to the same scale. For all experiments, n=3.

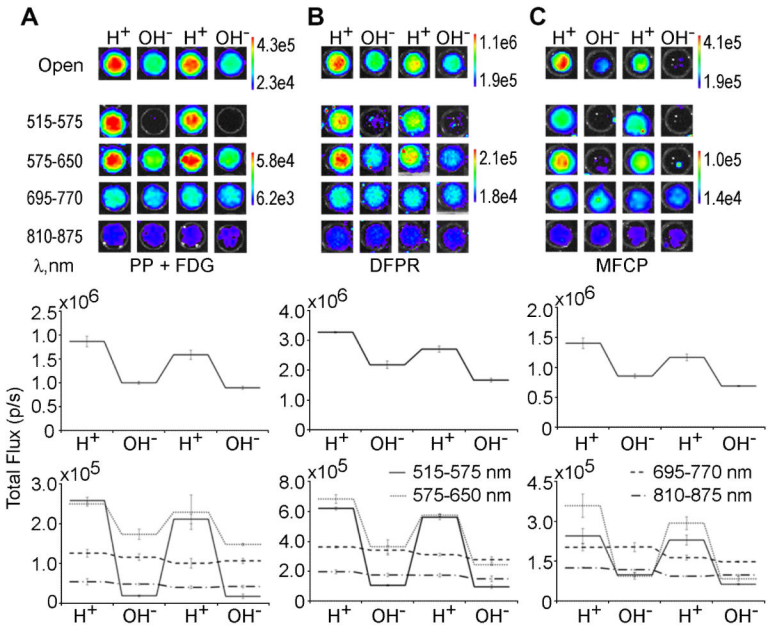

Figure 3. Optical switching of PP+^{18}F-FDG, ^{18}F-DFPR and ^{18}F-MFCP

10 μL of 1 M HCl (H^+) or NaOH (OH^-) was added to wells containing (A) 25 mM PP+200 μCi ^{18}F-FDG. (B) 200 μCi (50 nmol) ^{18}F-DFPR (λ_{max}=570 nm), and (C) 100 μCi (50 nmol) ^{18}F-MFCP (λ_{max}=582 nm) and images acquired after acid or base addition. Images for open and selective filters are shown on top, quantification of each well is shown below.

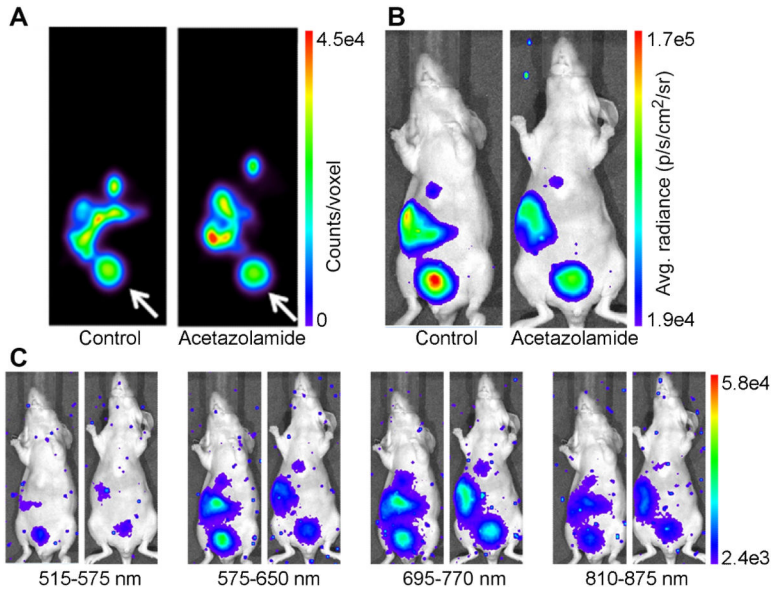

Figure 4. In vivo imaging of Cerenkov quenching

Mice were treated with either saline or 160 mg/kg acetazolamide for 5 days prior to imaging with ^{18}F-MFCP. (A) APET images of a single coronal slice 0.5 mm thick through the center of the mouse in control and acetazolamide-treated mice show ^{18}F-MFCP accumulation in bladder (white arrow), gall bladder, liver, intestine. Optical images of the same mice were acquired using (B) open filter and (C) the four emission filters.

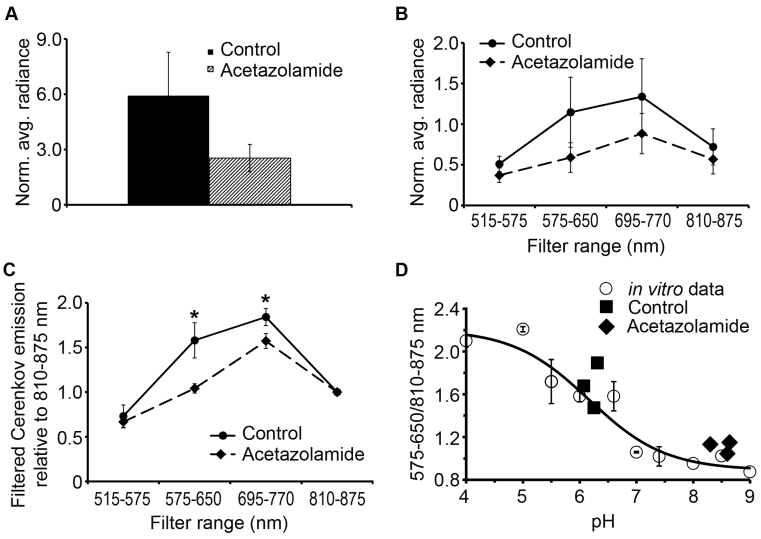

Figure 5. Quantification of in vivo Cerenkov images

Average radiance from the bladder using (A) open filter, (B) the 4 selective filters, (C) the ratio of emission at each filter relative to 810-875 nm. * significant, $p<0.05$, Students t-test, (D) Ratiometric pH determination. Open circles depict the ratio of Cerenkov emission at (575-650 nm)/(810-875 nm) for *in vitro* ^{18}F-MFCP (data from Figure 2C). The solid line is a fit to a sigmoidal curve and gives a pKa of 6.25, similar to 6.4 determined by the open filter data. Black diamonds and squares represent Cerenkov emission from control and acetazolamide-treated mice plotted against actual urine pH.

Table 1

Properties of Parent and F-labeled pH indicators

	Parent Compound		Mono-fluorinated		Di-fluorinated	
Indicator name	**pK_a**	**λ_{max}**	**pK_a**	**λ_{max}**	**pK_a**	**λ_{max}**
Phenol Red	7.9	558	7.3	564	6.4	570
Cresol Red	8.2	572	7.6	576	6.8	582
Cresol Purple	8.3	578	7.5	582	7.0	590
Phenolphthalein	9.7	553	9.3	558	8.7	564
Naptholphthalein	7.8	653	7.7	659	7.2	665

λ_{max} is the absorbance maximum of the basic form in nm.